Scientia Iranica C (2021) 28(3), 1353–1365

Sharif University of Technology
Scientia Iranica
Transactions C: Chemistry and Chemical Engineering
http://scientiairanica.sharif.edu

Heat-treated gilsonite as an efficient natural material for removing toluene: A Box-Behnken experimental design approach

A. Saffarian Delkhosh[a], A. Vahid[b], S. Baniyaghoob[a,*], and M. Saber-Tehrani[a]

a. *Department of Chemistry, Science and Research Branch, Islamic Azad University, Tehran, P.O. Box 14515-775, Iran.*
b. *Research Institute of Petroleum Industry (RIPI), West Blvd Azadi Sport Complex, Tehran, P.O. Box 14665-1998, Iran.*

Received 15 December 2019; received in revised form 1 January 2021; accepted 25 January 2021

KEYWORDS
Adsorption;
Toluene;
Experimental design;
Gilsonite;
Regeneration.

Abstract. Heat-Treated Gilsonite (HT-Gil) has been used for adsorptive removal of toluene from wastewater for years. In this respect, some appropriate standard test methods were employed to characterize the sample. The FT-IR spectrum was a proof of the presence of long aliphatic chains and aromatic rings. In addition, FE-SEM imaging was employed to investigate the surface morphology and grain size of the sample and confirm the irregular shape of the HT-Gil with different particle size distributions. The chemical properties and elemental composition of the sample were determined through several ASTM tests and XRF analysis. Moreover, TGA experimental results revealed the thermal stability of the sample at 350°C. Adsorption parameters including temperature (A: 5–45°C), pH (B: 4–9), and contact time (C: 20–90 min) were optimized using BBD. The results showed that the maximum adsorption capacity of 69.1% was achieved in an optimum condition featuring 5°C, pH 9, and 90 min. The used adsorbent had acceptable adsorption efficiency (62.12%) following four thermal regeneration cycles. Moreover, the results of equilibrium data were in accordance with those of the Freundlich isotherm model ($R^2 = 0.9531$) and revealed that the non-uniformity of the adsorbent surface was in line with that found previously in the literature.

1. Introduction

Volatile Organic Compounds (VOCs) encompass a wide range of carbon-containing gases and vapors which are mainly produced through the semiconductor manufacturing process and many other chemical processes containing hydrocarbon solvents [1,2]. VOCs, known as one of the major atmospheric pollutants, represent a distinct group of organic compounds with a Reid vapor pressure of 0.01 kPa or higher that can readily evaporate at room temperature [3–5]. Different hazardous effects of VOCs on the environment and human health including the formation of ground-level ozone, fine particulate matt ($PM_{2.5}$), photochemical smog, and Secondary Organic Aerosols (SOAs) have been already reported in the literature [6–8]. A prominent member of VOCs, toluene (methylbenzene) is a clear, colorless, volatile, flammable liquid of low viscosity and explosive nature in the air with a benzene-like odor [9]. This aromatic hydrocarbon causes severe health-related problems involving respiratory

*. *Corresponding author.*
E-mail address: baniyaghoob@gmail.com (S. Baniyaghoob)

doi: 10.24200/sci.2021.55043.4043

diseases, failure of the liver, kidneys, central nervous system, and even cancer at very low concentration levels (< 100 ppmv) [10,11]. Therefore, a number of countries and regions have introduced stringent regulations to control the VOC emissions from polluting industries by imposing strict emission standards in recent years [12]. Nowadays, a number of techniques such as adsorption [13,14], absorption [15], catalytic oxidation [16], catalytic combustion [17], photocatalytic oxidation [18], condensation [19], and biofiltration [20] have been employed to remove VOCs. Among all the mentioned techniques, adsorption is broadly utilized and considered as a simple, efficient, cost-effective, and eco-friendly process in eliminating VOCs, particularly in low concentrations [12,21]. To this end, many types of adsorbents including Activated Carbon (AC) [22], zeolites [23], silica gel [24], aerogel [25], alumina [26], and Metal-Organic Frameworks (MOFs) [27] have been applied to the process of adsorptive removal of VOCs. For instance, AC is usually used as the most common adsorbent owing to its high specific surface area, microporous structure as well as functional groups, and high availability. However, it has a number of drawbacks: flammability risk, low thermal stability, blocked pores, difficult regeneration, and hygroscopicity. However, other common commercial adsorbents such as zeolites and alumina are often expensive or cause low adsorption capacity problems [1,28]. Hence, the necessity of introducing new adsorption materials to eliminate VOCs is highlighted.

Gilsonite, scientifically known as "uintahite", is a natural solid hydrocarbon discovered in the 1860s in the Uinta Basin, Utah (USA) mined in underground shafts. Gilsonite has a brilliant and obsidian-like appearance that is readily pulverized into dark brown powder. Due to its unique chemical and physical properties, gilsonite is widely used in mining and other different industrial applications such as production of asphalt binder modifiers, oil drilling fluids, paint products, enamels, inks, and so on [29–31].

The objective of this study is to introduce Heat-Treated Gilsonite (HT-Gil) as a new type of natural adsorbent used for removing toluene, as a representative of VOCs, from aqueous media. In addition, characterization of the sample was carried out by Fourier Transform Infrared (FT-IR) spectroscopy, X-Ray Diffraction (XRD), X-Ray Fluorescence (XRF) spectrometry, Thermo-Gravimetric Analysis (TGA), and Field Emission Scanning Electron Microscopy (FE-SEM) techniques. The effects of significant parameters including temperature, pH, and contact time were determined using a three-level, three-variable Box-Behnken Design (BBD) from Response Surface Methodology (RSM) using the Design Expert® Version 7.0 (StatEase Inc., USA). Moreover, the regeneration processes were performed using solvent washing and thermal recycling. Finally, Langmuir, Freundlich, and Temkin isotherm models were employed to analyze the experimental equilibrium data.

2. Experimental

2.1. Preparation and characterization of HT-Gil

The gilsonite samples used in this study were collected from a gilsonite mine in Kermanshah Province, situated in the West of Iran. All of the samples were pulverized and sieved through a 200-mesh sieve. In order to remove the trapped water molecules and low-boiling species, the resultant powder was heated in a vacuum oven at 180°C and 5 mmHg for 1 h.

2.2. Characterization

The FT-IR spectrum (KBr pellet method) was obtained through a Thermo Nicolet Nexus 870 FT-IR spectrometer at room temperature. The surface morphology of HT-Gil was evaluated using scanning electron microscopy (TESCAN, MIRA3 XMU) operating at 15 kV. The XRD pattern was obtained through a Seifert XRD 3003 PTS diffractometer with CuKα X-ray radiation (λ = 1.54 Å). Thermo-Gravimetric Analysis (TGA) was carried out using a Mettler Toledo TGA/SDTA 851 apparatus under argon (Ar) atmosphere at a ramping rate of 10°C min^{-1} and temperatures ranging from the ambient temperature to 950°C. The quantitative elemental analysis of the sample was conducted using an X-ray fluorescence spectrometer (RIGAKU ZSX Primus IV). The physical properties and elemental analysis of the treated sample are summarized in Table 1. Toluene concentration was analyzed by a UV-Vis spectrophotometer (Varian Cary 300) at λ_{max} of 261 nm. Moreover, the solutions were centrifuged using a Hettich Rotofix 32A centrifuge.

Table 1. Physical properties and elemental analysis of HT-Gil.

Properties	Test method	Results (%)
Ash content	ASTM D3174	6.2
Moisture content	ASTM D3173	1.3
Solubility in TCE	ASTM D2042	89.1
Carbon content	ASTM D5291	77.9
Hydrogen content	ASTM D5291	7.9
Nitrogen content	ASTM D5291	0.9
Calcium content	XRF	0.18
Iron content	XRF	0.018
Sulfur content	XRF	11.76
Nickel content	XRF	Trace
Vanadium content	XRF	0.024
Strontium content	XRF	0.012

Table 2. The physico-chemical properties of toluene [33–38].

Property	Value
Formula	C_7H_8
Molar mass (g mol^{-1})	92.14
Boiling point (°C)	110.6
Melting point (°C)	-94.9
Kinetic diameter (nm)	0.56
Polarizability (Å^3)	11.86
Relative density (g L^{-1})	0.86
Saturated vapor pressure at 30°C (kPa)	4.89
Solubility in water at 20°C (g L^{-1})	515
Dipole moment (Debye)	0.33
Ionization energy (eV)	8.83
Henry's law constant (unitless)	0.24

2.3. Batch adsorption experiments

The ability of HT-Gil as a natural adsorbent to remove toluene from aqueous media was investigated in a batch process. The physical and chemical properties of toluene are presented in Table 2. Prior to adsorption experiments, the adsorbent was degassed at 100°C in a vacuum oven overnight and stored in a desiccator. Then, the stock solution of toluene with a concentration of 1000 mg L^{-1} was prepared through double distilled-deionized water and diluted to the required concentrations for each of the adsorption experiments. In this study, a temperature-controlled reciprocating shaker was set to operate at 200 rpm, and 100-ml glass Erlenmeyer flasks with PTFE-lined screw cap were utilized in all experiments. Batch optimization experiments were conducted using 50 mL of toluene solutions with an initial concentration of 100 mg L^{-1} and a definite amount (200 mg) of the adsorbent. Furthermore, the pH values for the solutions were adjusted using 0.05 M NaOH or 0.05 M H_2SO_4. To elaborate the adsorption mechanism, isotherm studies were conducted under some optimal conditions using 4 g L^{-1} of the adsorbent and the solution with initial toluene concentration ranging from 25 to 100 mg L^{-1}. After the adsorption process, the solutions were centrifuged at 6000 rpm and the supernatant was filtered by a filter paper with a pore size of 0.45-μm and immediately analyzed by a UV-Vis spectrophotometer. The toluene removal percentage and adsorption capacity (q_e, mg g^{-1}) were determined using Eqs. (1) and (2), respectively [32]:

$$\text{Removal } (\%) = \frac{100(C_0 - C_e)}{C_0}, \tag{1}$$

$$q_e = \frac{(C_0 - C_e)v}{m}, \tag{2}$$

where C_0 is the initial toluene concentration (mg L^{-1}), C_e the equilibrium concentration of toluene in solution (mg L^{-1}), v the volume of the liquid phase in liter, and m the dry weight of adsorbent in gram.

2.4. Box-Behnken statistical design of experiment

BBD, a very appealing design for the RSM model, is a powerful and up-to-date method for optimizing the process conditions, categorized into a rotatable or nearly rotatable second-order design on the basis of three-level incomplete factorial designs [39]. A three-level three-variable BBD in some conditions including temperatures A (5, 25, and 45°C), pH, B (4, 6.5, and 9), and contact times C (20, 55, and 90 min) was employed to determine the main effects of the variables on the toluene adsorption by the proposed adsorbent. The main variables with three levels (the high, low, and central points of factors were coded as +1, –1, and 0, respectively) are presented in Table 3.

The actual variables (X_i) were coded based on linear transformation according to Eq. (3):

$$x_i = \frac{X_i - \frac{(X_{\text{high}} + X_{\text{low}})}{2}}{\frac{X_{\text{high}} + X_{\text{low}}}{2}}, \tag{3}$$

where x_i is the dimensionless coded value of the ith independent variable and X_i is the uncoded value of the ith independent variable. In addition, X_{high} and X_{low} are the high and low levels of uncoded factors, respectively [40].

The total number of 17 experiments (N) were conducted to develop BBD consisting of 12 factorial points and 5 center points.

$$N = 2k(k-1) + c, \tag{4}$$

$$N = 2 \times 3 \times (3-1) + 5 = 17, \tag{5}$$

where k is the number of independent variables and c is the number of center points [41].

The mathematical relationship between the variables and responses was illustrated by the following second-order polynomial equation (Eq. (6)), which is a function of independent variables, interactions, and squared terms:

$$Y = \beta_0 + \sum_{i=1}^{k} \beta_i x_i + \sum_{i=1}^{k} \beta_{ii} x_i^2 + \sum_{i=1}^{k} \sum_{i \prec j}^{k} \beta_{ij} x_i x_j + \varepsilon. \tag{6}$$

Table 3. Independent variables and coded levels for the BBD design.

Variables	Symbol	Level		
		−1	0	+1
Temperature (°C)	A	5	25	45
pH	B	4	6.5	9
Contact time (min)	C	20	55	90

Here, Y is the predicted response (i.e., toluene removal percentage); x_i and x_j are the coded independent variables; β_0 is the offset term; β_i, β_{ii}, and β_{ij} are linear, quadratic, and interaction coefficients, respectively. Further, i and j are the index numbers of variables, and ε represents the residual error [42,43].

3. Results and discussion

3.1. Characterization

FT-IR spectroscopy was employed in this study to identify the functional groups on the surface of the mineral materials. Figure 1 shows the FT-IR spectrum for the HT-Gil sample in the wavenumber ranging from 3700 to 500 cm^{-1}. In Figure 1, two very strong peaks at 2918 and 2852 cm^{-1} are assigned as asymmetric and symmetric C-H stretching vibrations, respectively. The intensity of the peak at 2918 cm^{-1} corroborates the presence of long aliphatic chains in the respective sample. The appearance of an sp^2 aromatic band in the region of 3000-3100 cm^{-1} results from the C-H stretching modes. The peak observed at 2357 cm^{-1} is possibly related to the C=O stretching vibrations of ambient CO_2 molecules. The peak observed at 1585 cm^{-1} is caused by the stretching vibrations of C=C in the aromatic rings. The peaks 1450 and 1370 cm^{-1} are related to the bending vibrations of asymmetric C-CH_3 bonds and/or CH_2 and symmetric C-CH_3 bonds. The high-intensity band at 1023 cm^{-1} is attributed to the sulfoxide group. Medium intensity bands between 730 and 850 cm^{-1} wavenumbers originated from C-H out-of-plane bending vibrations of aromatic compounds. The broadband centered around 3450 cm^{-1} is also visible in the IR spectrum and corresponds to N-H or O-H groups [44–49].

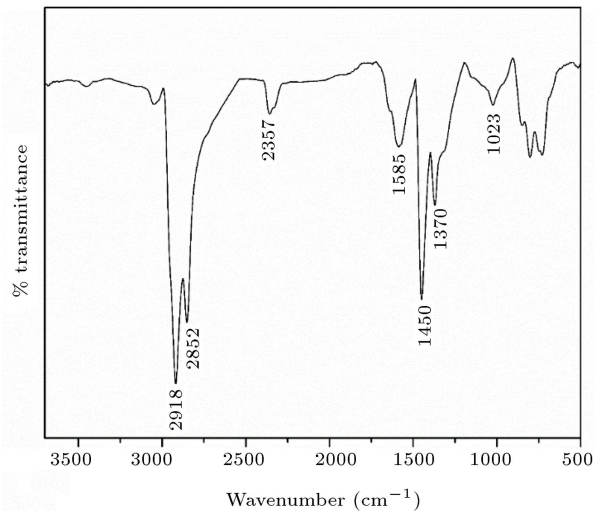

Figure 1. FT-IR spectrum of HT-Gil.

The FE-SEM, a significant sort of electron microscopical technique, is a promising tool for generating high-resolution images of micro/nano-materials through high-energy electron beams and provides useful data about particle size distribution and surface morphology of different samples [50,51]. The surface morphology of HT-Gil is characterized by FE-SEM images, as depicted in Figure 2. As observed, the sample is characterized by a porous structure with different particle size distributions, and it appears that the particles have polyhedral shapes with a relatively smooth surface morphology.

The XRD pattern of HT-Gil at 2θ ranges from 10° to 80°, as shown in Figure 3. No sharp peaks are observed in the XRD pattern, which is indicative of the amorphous nature of HT-Gil. The diffractogram contains two very broad and weak peaks at 2θ angles around 23° and 43°, which are related to the diffraction planes of (d_{002}) and (d_{010}), respectively. While the peak appearing at 23° is attributed to crystalline regions of diffraction from the layering of graphitic carbons, that at 43° corresponds to the formation

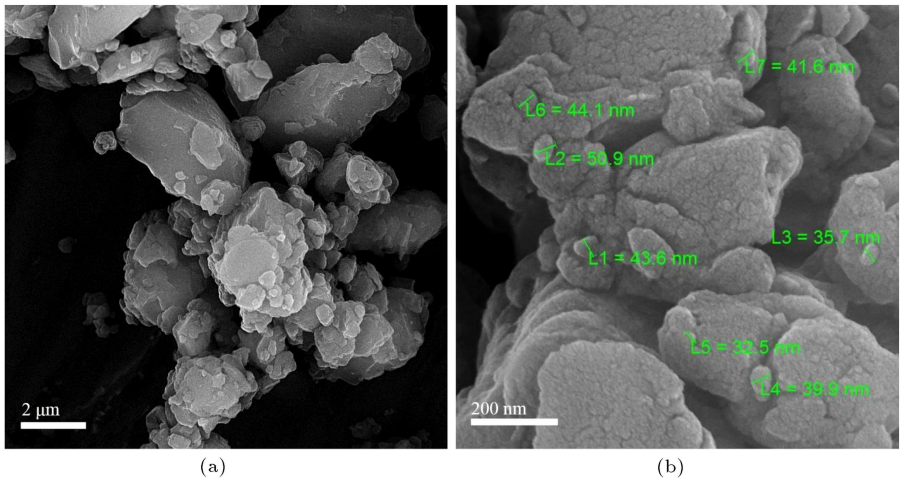

(a) (b)

Figure 2. (a) Low- and (b) high-magnification FE-SEM images of HT-Gil.

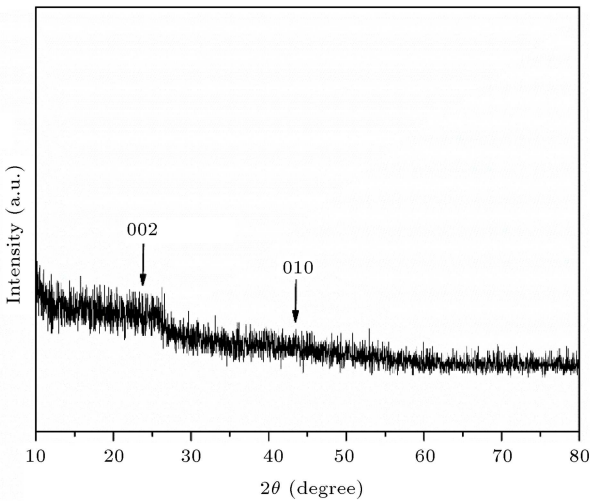

Figure 3. Wide-angle X-ray pattern of HT-Gil.

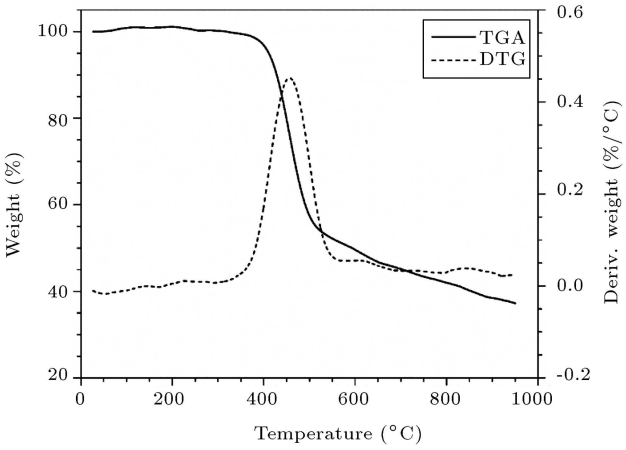

Figure 4. TGA/DTG analysis curves for HT-Gil sample under argon atmosphere.

of small 2D lattices. To be specific, the sample is characterized by small crystallinity produced by the sp^2-hybridized graphitic system according to the XRD analysis [45,52].

Thermo-Gravimetric Analysis (TGA) is a simple analytical method that determines the thermal stability and fraction of volatile components of a material by measuring the weight variations for the sample when exposed to heat at a constant rate [53]. Figure 4 shows the profiles of TGA and Derivative Thermo-Gravimetric (DTG) analysis of the HT-Gil sample with a heating rate of 10°C min^{-1}. The TGA curve shows one single stage of weight loss about 52% w/w between 350°C and 550°C. Moreover, the DTG curve of the sample exhibited one distinct peak centered at 456°C corresponding to the maximum weight loss rate. The mass loss of the specimen is mainly attributed to the decomposition (pyrolysis) and volatilization of hydrocarbon compounds. The weight loss of the sample continued marginally above 550°C. In addition, the amount of solid residue at the final temperature of 950°C was 37% w/w.

3.2. Experimental design methodology

A three-level three-variable BBD from RSM was employed to determine the optimal removal efficiency of toluene (representative of VOCs) from aqueous media. BBD matrix with three factors consisting of 17 experimental runs and 5 replicates at the center point was investigated, the results of which are summarized in Table 4.

According to the statistics of the model summary (Table 5), the cubic model was found to be statistically aliased, and 2-Factor Interaction (2FI) model had the highest values of adjusted determination coefficient (Adj R-Sq = 0.896) and predicted determination coefficient (Pred R-Sq = 0.8246). Consequently, the 2FI model was selected for further analysis.

The results of the Analysis of Variance (ANOVA) statistical method are presented in Table 6. Generally, the proposed model and its corresponding terms with p-values smaller than 0.05 are highly significant at a confidence interval of 95%. In this respect, in the 2FI model, although independent variables of A and B and all the interaction terms (i.e., AB, AC, and BC) are statistically significant, C is not significant ($p - \text{value} > 0.05$). Among the model terms, AC and C terms with F-values of 61.29 and 0.17 have the most and the least impacts on the response, respectively. Furthermore, the Lack Of Fit (LOF) of the model was not as significant as the F-value of 0.44, and the p-value was more than 0.05 (0.8267).

The final equation calculated in terms of the coded variables can be expressed by the following equation:

$$\text{Removal } (\%) = 59.56 - 2.24A + 2.11B - 0.25C - 3.95AB - 6.73AC + 5.12BC. \quad (7)$$

The 3D surface and 2D contour plots in Figure 5 indicate the relationship of each of the input variables with the removal efficiency of toluene. Figure 5(a) illustrates the interactive effects of pH and temperature parameters. As observed, the amount of toluene adsorption increased gently with increasing temperature from 5°C to 45°C. Figure 5(b) depicts the interaction between the contact time and pH. The removal efficiency of toluene slightly decreased by increasing the contact time in the acidic pH range. On the contrary, at basic pH values, upon increasing the contact time, the removal percentage rose dramatically. Therefore, it can be concluded that the contact time is less significant than the pH value in terms of the response. The combined effect of the contact time and temperature is shown in Figure 5(c). The toluene removal efficiency slightly increases upon increasing the temperature and

Table 4. Box-Behnken design matrix and experimental responses.

Run no.	Independent variables			Removal (%)
	***A*: Temperature (°C)**	***B*: pH**	***C*: Contact time (min)**	
1	5	4	55	55.6
2	45	4	55	58
3	5	9	55	69.1
4	45	9	55	55.7
5	5	6.5	20	54
6	45	6.5	20	64
7	5	6.5	90	66.7
8	45	6.5	90	49.8
9	25	4	20	64.1
10	25	9	20	56.7
11	25	4	90	53.6
12	25	9	90	66.7
13	25	6.5	55	59.2
14	25	6.5	55	62.6
15	25	6.5	55	57.9
16	25	6.5	55	61.1
17	25	6.5	55	57.7

Table 5. Model summary statistics.

Source	Std. Dev.	R-Sq	Adj R-Sq	Pred R-Sq	PRESS
Linear	5.39	0.1679	–0.0241	–0.7037	773.7
2FI	1.72	0.935	0.896	0.8246	79.64
Quadratic	1.85	0.9474	0.8799	0.7269	124.03
Cubic	2.11	0.9607	0.8427		+

Table 6. Analysis of variance table for response surface 2FI model.

Source	Sum of squares	*df*	Mean square	*F*-value	*p*-value $Prob > F$
Model	424.63	6	70.77	23.98	< 0.0001
A: Temperature	40.05	1	40.05	13.57	0.0042
B: pH	35.7	1	35.7	12.1	0.0059
C: Contact time	0.5	1	0.5	0.17	0.6893
AB	62.41	1	62.41	21.15	0.001
AC	180.9	1	180.9	61.29	< 0.0001
BC	105.06	1	105.06	35.6	0.0001
Residual	29.51	10	2.95		
Lack of fit	11.65	6	1.94	0.44	0.8267
Pure error	17.86	4	4.47		
Cor total	454.14	16			

the curvature of the response surface is clearly visible. Moreover, the maximum adsorption capacity of 69.1% is obtained at 5°C, pH 9, and 90 min.

3.3. Regeneration of HT-Gil

Reusability of the adsorbent is regarded as an integral parameter for assessing its efficiency, especially for commercial applications. Prior to the regeneration process, HT-Gil was saturated in a toluene solution (at a constant concentration of 100 mg L^{-1}) under an optimum adsorption condition and then, collected after filtration. The regeneration process was implemented

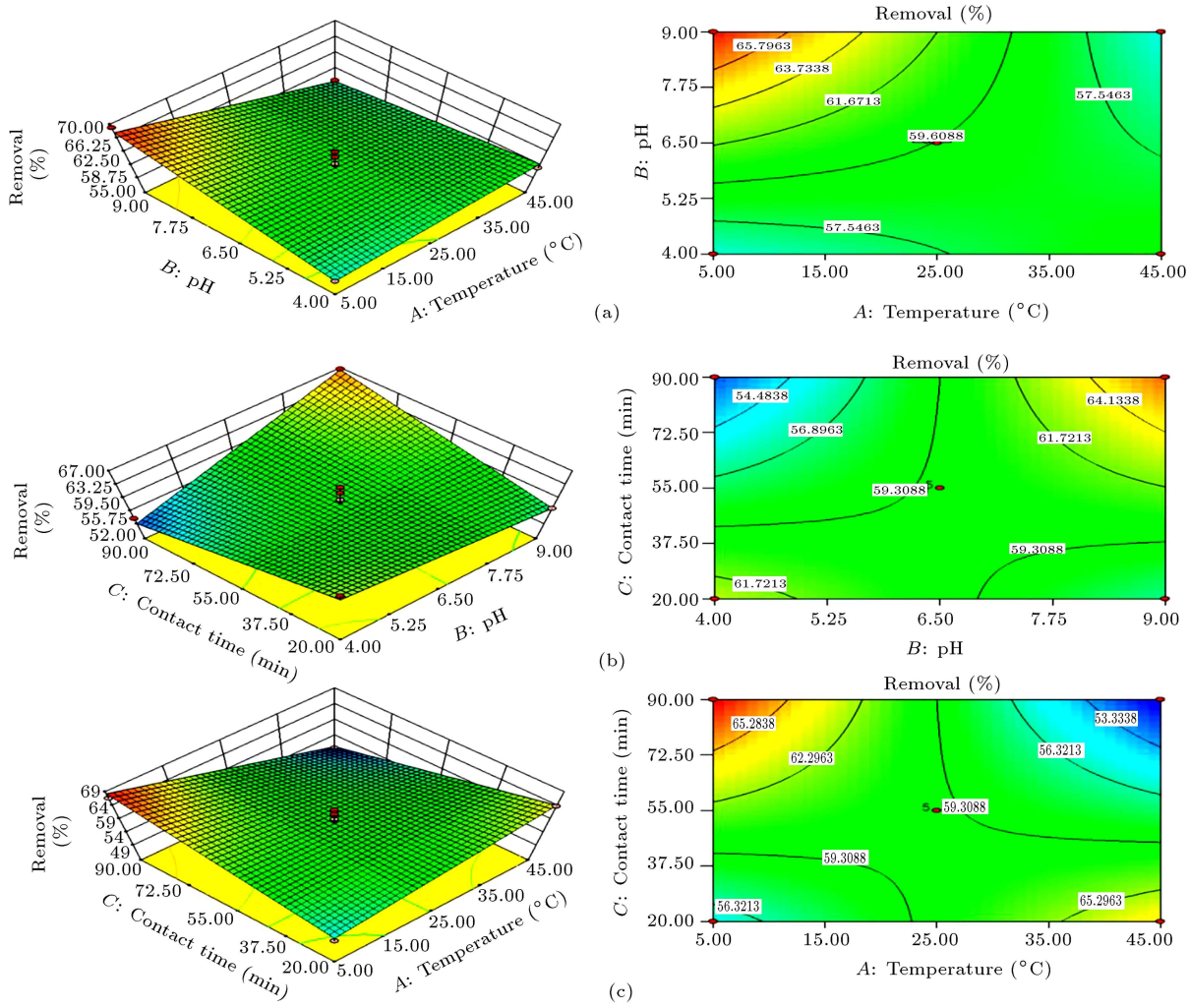

Figure 5. 3D surface and 2D contour plots of toluene removal as a function of (a) temperature vs. pH (contact time = 55 min), (b) pH vs. contact time (temperature = 25°C), and (c) temperature vs. contact time (pH = 6.5).

through solvent washing (10 mL, including ethanol and acetone) and thermal regeneration (calcination at 250°C for 20 min). As presented in Figure 6(a), the removal efficiency of the recycled HT-Gil after applying the regeneration methods is of the following order: thermal regeneration > acetone washing > ethanol washing. As a result, the thermal regeneration method was chosen for the next four regenerative cycles. According to Figure 6(b), the regenerated adsorbent caused a slight reduction in the adsorption capacity of toluene after four adsorption-regeneration cycles. This reduction might be related to the blocked pores of adsorbent by agglomerates of decomposed products during each regeneration cycle.

3.4. Adsorption isotherms

In this study, three common isotherm models including Langmuir, Freundlich, and Temkin were employed to fit the equilibrium adsorption data. In the Langmuir model, all of the adsorption sites are active, the surface is homogenous, only a monolayer surface with no attraction of adsorbate is formed through the adsorption process, and each adsorbate has equal sorption [54]. The linear equation of the Langmuir model is given in the following (Eq. (8)):

$$\frac{C_e}{q_e} = \frac{C_e}{q_m} + \frac{1}{K_L q_m}, \tag{8}$$

where q_m (mg g^{-1}) is the theoretical monolayer saturation capacity, K_L (L mg^{-1}) is the Langmuir constant, and q_e (mg/g) and C_e (mg/L) are the amount of adsorbed per unit weight of adsorbent and unadsorbed adsorbate in solution in the equilibrium concentration, separately. To clarify the adsorption process, a dimensionless constant separation factor equilibrium parameter (R_L) is presented (Eq. (9)):

$$R_L = \frac{1}{1 + K_L C_i}, \tag{9}$$

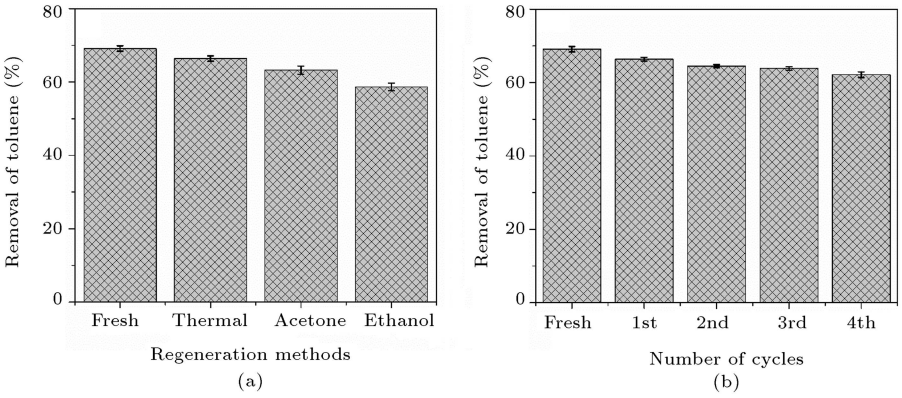

Figure 6. (a) Regeneration of spent HT-Gil through several regeneration procedures. (b) Removal capacities of the regenerated HT-Gil by thermal regeneration method up to four regeneration cycles.

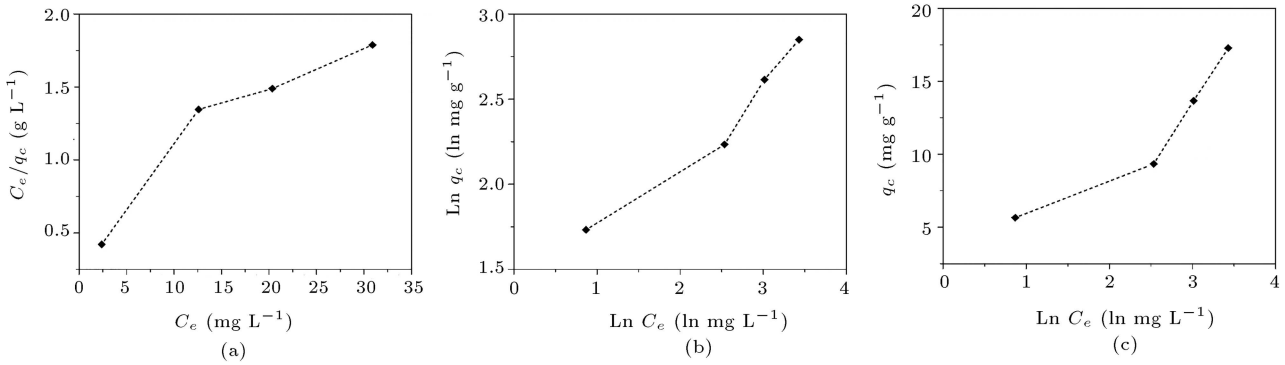

Figure 7. (a) Langmuir, (b) Freundlich, and (c) Temkin isotherm plots for adsorption of toluene onto HT-Gil.

where K_L (L mg^{-1}) is the Langmuir constant and C_i (mg L^{-1}) is the initial concentration of adsorbate. The value of R_L determines that whether the adsorption process is unfavorable ($R_L > 1$), linear ($R_L = 1$), favorable ($0 < R_L < 1$), or irreversible ($R_L = 0$) [55,56].

In the Freundlich isotherm, the interaction between the adsorbate and the surface sites is observable. Consequently, at the ending point of the adsorbent, the adsorption energy decreases exponentially. The linearized form of the Freundlich equation is as follows:

$$\ln q_e = \ln K_F + \frac{1}{n} \ln C_e, \tag{10}$$

where K_F (mg g^{-1}) and n are the Freundlich constants denoting the adsorption capacity and adsorption intensity, respectively. The degree of non-linearity of solution concentration and adsorption was determined by the n value. The adsorption process can be linear ($n = 1$), chemical ($n < 1$), or favorable physical process ($n > 1$) [56,57].

In the Temkin isotherm model, the adsorption heat of the molecules declined linearly with the coverage of the surface. The adsorption process is determined by the homogenous dispensation of binding energies up to the highest binding energies. The linear form of the Temkin model is defined as (Eq. (11)):

$$q_e = B_T \ln K_T + B_T \ln C_e, \tag{11}$$

where B_T and K_T (L mg^{-1}) are the heat of adsorption and Temkin isotherm constant, q_e is the amount of adsorbate in the adsorbent at equilibrium, and C_e is equilibrium concentration [57,58]. Adsorption isotherm model plots are depicted in Figure 7(a)–(c). The related parameters for each model are presented in Table 7. A comparison of regression coefficient (R^2) values from these models showed that the equilibrium data were well adapted to the Freundlich model (the highest R^2 value of 0.9531). The n value in the Freundlich equation was 2.3590 ($n > 1$) which was indicative of favorable physisorption. The maximum adsorption capacity was measured as 21.8341. Moreover, the R_L value from Langmuir isotherm was between 0 and 1, suggesting a favorable adsorption process.

Thermalization of untreated gilsonite (extracted gilsonite) contributes to removing oils and obtaining stable pores after cooling to room temperature. This process causes a decrease in the relative amounts of functional groups containing oxygen due to evaporation. According to the results of FT-IR and XRD, the heat treatment operation is a vital process in

Table 7. Langmuir, Freundlich, and Temkin isotherm model constants and correlation coefficients.

Isotherm model	Parameters	Values
Langmuir	q_m (mg g^{-1})	21.8341
	K_L (L mg^{-1})	0.0910
	R^2	0.8779
	R_L	0.0990–0.3053
Freundlich	K_F (mg g^{-1})	3.7216
	n	2.3590
	R^2	0.9531
Temkin	K_T (L mg^{-1})	1.3040
	B_T	4.2107
	R^2	0.8733

forming carbon-rich polycyclic aromatic hydrocarbons as high-boiling species. Consequently, the adsorption of toluene by HT-Gil is probably related to the π-π interaction of the aromatic ring of toluene with residual aromatic hydrocarbons in the pores of the sorbent [45,52]. In addition, Table 8 compares the toluene adsorption capacity of HT-Gil with those of some other adsorbents previously reported in the literature.

4. Conclusion

HT-Gil was introduced as a low-cost natural adsorbent used for the removal of toluene from aqueous solution. Different surface chemical functional groups confirmed the amorphous structure of HT-Gil with small crystallinity from the sp^2-hybridized graphitic system, which would cause $\pi-\pi$ interactions of toluene onto the HT-Gil during the adsorption process. BBD technique under RSM was selected to optimize the adsorption process. The effects of temperature, pH, and contact time as three different variables on the response were also investigated. According to the results obtained from ANOVA analysis, the validity and accuracy of the 2FI model based on an F-value of 23.98, $p-$value $<$ 0.0001, and insignificant LOF were confirmed. Among independent variables and interactions, AC with an F-value of 61.29 and C with an F-value of 0.17 had the most and the least effects on the response, respectively. The proposed adsorbent enjoyed another advantage, i.e., simple regeneration by thermal regeneration at a relatively moderate temperature or by solvent washing. The Freundlich adsorption isotherm model was well fitted to the experimental data. The calculated Freundlich constant n was larger than unity, and the physical adsorption was the most favorable adsorption mechanism. The obtained results indicated that natural gilsonite was an appropriate candidate for removing hazardous chemicals from wastewater in terms of cost-effectiveness, efficiency, and mild technical condition. This new type of adsorbent can be employed to eliminate harmful organic compounds, which cannot be easily removed by conventional adsorbents such as some activated carbons and zeolites.

Table 8. Comparison of adsorption capacities of various adsorbents for adsorptive removal of toluene from aqueous media.

Adsorbents	Adsorption capacity q_e (mg g^{-1})	Conditions	Ref.
HT-Gil	21.83[a]	pH : 9, T : 5	Present work
APCNTs	23.28	pH : 6, T : 20	[59]
CNTs-5.9%	31.28	pH : 7, T : 20	[59]
Nano-Fe	9.8	pH : 7, T : 10, C_0 : 10	[60]
Hybrid CNT	9.95	pH : 7, T : 10, C_0 : 10	[60]
HCNT (MWCNT-SiO_2)	9.96	pH : 7, T : 10	[61]
OMC	18.2	pH : 7, T : 25, C_0 : 10	[62]
Thermally treated lignite	0.0343[b]	pH : 5, T : 20	[63]
Activated carbon (date-palm pits)	5.53[a]	pH : 10, T : 20	[64]
Activated carbon (olive stones)	5.8	pH : 7.8, T : 25	[65]
Activated carbon (cotton stalks)	6.7	pH : 7.8, T : 25	[65]
Smectite organoclay	1.27[a]	pH : 9, T : 24	[66]
Sericite mica	16[a]	pH : 7.7, T : 20	[61]
MWCNT	9.8	pH : 7, T : 10, C_0 : 10	[60]

Note: T = temperature (°C); C_0 = initial concentration (mg L^{-1});

MWCNT = Multi-Walled Carbon Nanotube; OMC = Ordered Mesoporous Carbon;

[a]: Maximum adsorption capacity (mg g^{-1});

[b]: mmol g^{-1}.

Acknowledgements

This work was supported by research funds from Iran Nanotechnology Innovation Council (Grant Nos. 110138 and 137952). The authors are grateful for the supporting facilities from the Zakariya Razi Laboratory Complex, Science and Research Branch, Islamic Azad University. Furthermore, we would also like to express our sincere gratitude to Dr. Nima Mohammadi for his cooperation in the laboratory and to Dr. Shadi Ghezelbash for her informative discussions and assistance with editing the manuscript.

References

1. Jafari, S., Ghorbani-Shahna, F., Bahrami, A., et al. "Adsorptive removal of toluene and carbon tetrachloride from gas phase using zeolitic imidazolate framework-8: Effects of synthesis method, particle size, and pretreatment of the adsorbent", *Microporous and Mesoporous Materials*, **268**, pp. 58–68 (2018).
2. Su, J., Bae, J., Park, S., et al. "Plasma-assisted oxidation of toluene over Fe/zeolite catalyst in DBD reactor using adsorption/desorption system", *Catalysis Communications*, **113**(May), pp. 36–40 (2018).
3. Niu, J., Qian, H., Liu, J., et al. "Process and mechanism of toluene oxidation using $Cu_{1-y}Mn_2Ce_yO_x$/sepiolite prepared by the co-precipitation method", *Journal of Hazardous Materials*, **357**, pp. 332–340 (2018).
4. Cheng, Z., Chen, Z., Li, J., et al. "Mesoporous silica-pillared clays supported nanosized Co_3O_4-CeO_2 for catalytic combustion of toluene", *Applied Surface Science*, **459**, pp. 32–39 (2018).
5. Shahzad, M., Razzak, S.A., Hossain, M.M., et al. "Catalytic oxidation of volatile organic compounds (VOCs)-A review", *Atmospheric Environment*, **140**, pp. 117–134 (2016).
6. Wang, H., Lu, Y., Han, Y., et al. "Enhanced catalytic toluene oxidation by interaction between copper oxide and manganese oxide in Cu-O-Mn/γ-Al_2O_3 catalysts", *Applied Surface Science*, **420**, pp. 260–266 (2017).
7. Feng, X., Guo, J., Wen, X., et al. "Enhancing performance of Co/CeO_2 catalyst by Sr doping for catalytic combustion of toluene", *Applied Surface Science*, **445**, pp. 145–153 (2018).
8. Luo, Y., Zheng, Y., Zuo, J., et al. "Insights into the high performance of Mn-Co oxides derived from metal-organic frameworks for total toluene oxidation", *Journal of Hazardous Materials*, **349**(January), pp. 119–127 (2018).
9. Abri, R.G.F., Ag, V., Fabri, J., et al. "Toluene", *Ullmann's Encyclopedia of Industrial Chemistry* (2000).
10. Dizbay-onat, M., Floyd, E., Vaidya, U.K., et al. "Applicability of industrial sisal fiber waste derived activated carbon for the adsorption of volatile organic compounds (VOCs)", *Fibers and Polymers*, **19**(4), pp. 805–811 (2018).
11. Kim, J.M.H., Lee, C.Y., Jerng, D.W., et al. "Toluene and acetaldehyde removal from air on to graphene-based adsorbents with microsized pores", *Journal of Hazardous Materials*, **344**, pp. 458–465 (2018).
12. Wang, X., Ma, C., Xiao, J., et al. "Benzene/toluene/water vapor adsorption and selectivity of novel C-PDA adsorbents with high uptakes of benzene and toluene", *Chemical Engineering Journal*, **335**, pp. 970–978 (2018).
13. Zhang, A.X., Yang, Y.Y., Song, L., et al. "Enhanced adsorption performance of gaseous toluene on defective UiO-66 metal organic framework: Equilibrium and kinetic studies", *Journal of Hazardous Materials*, **365**, pp. 597–605 (2019).
14. Yu, L., Wang, L., Xu, W., et al. "Adsorption of VOCs on reduced graphene oxide", *Journal of Environmental Sciences*, **67**, pp. 171–178 (2018).
15. Lalanne, F., Malhautier, L., Roux, J.-C., et al. "Absorption of a mixture of volatile organic compounds (VOCs) in aqueous solutions of soluble cutting oil", *Bioresource Technology*, **99**(6), pp. 1699–1707 (2008).
16. Li, Y., Liu, F., Fan, Y., et al. "Silver palladium bimetallic core-shell structure catalyst supported on TiO_2 for toluene oxidation", *Applied Surface Science*, **462**, pp. 207–212 (2018).
17. Wang, Q., Yeung, K.L., and Bañares, M.A. "Ceria and its related materials for VOC catalytic combustion: A review", *Catalysis Today*, **356**(1), pp. 141–154 (Oct. 2020).
18. Mamaghani, A.H., Haghighat, F., and Lee, C.S. "Gas phase adsorption of volatile organic compounds onto titanium dioxide photocatalysts", *Chemical Engineering Journal*, **337**, pp. 60–73 (2018).
19. Belaissaoui, B., Le Moullec, Y., Favre, E., et al. "Energy efficiency of a hybrid membrane/condensation process for VOC (volatile organic compounds) recovery from air: A generic approach", *Energy*, **95**, pp. 291–302 (2016).
20. Cheng, Y., He, H., Yang, C., et al. "Challenges and solutions for biofiltration of hydrophobic volatile organic compounds", *Biotechnology Advances*, **34**(6), pp. 1091–1102 (2016).
21. Qiao, N., He, C., Zhang, X., et al. "Hollow mesoporous silica materials with well-ordered cubic Ia3d mesostructured shell for toluene adsorption", *Journal of Porous Materials*, **26**(1), pp. 59–68 (2019).
22. Baur, G.B., Beswick, O., Spring, J., et al. "Activated carbon fibers for efficient VOC removal from diluted streams: the role of surface functionalities", *Adsorption*, **21**(4), pp. 255–264 (2015).
23. Kraus, M., Trommler, U., Holzer, F., et al. "Competing adsorption of toluene and water on various zeolites", *Chemical Engineering Journal*, **351**, pp. 356–363 (2018).

24. Sui, H., An, P., Li, X., et al. "Removal and recovery of o-xylene by silica gel using vacuum swing adsorption", *Chemical Engineering Journal*, **316**, pp. 232–242 (2017).

25. Maleki, H. "Recent advances in aerogels for environmental remediation applications: A review", *Chemical Engineering Journal*, **300**, pp. 98–118 (2016).

26. Chen, D., Qu, Z., Sun, Y., et al. "Adsorption-desorption behavior of gaseous formaldehyde on different porous Al_2O_3 materials", *Colloids and Surfaces A: Physicochemical and Engineering Aspects*, **441**, pp. 433–440 (2014).

27. Chu, F., Zheng, Y., Wen, B., et al. "Adsorption of toluene with water on zeolitic imidazolate framework-8/graphene oxide hybrid nanocomposites in a humid atmosphere", *RSC Advances*, **8**(5), pp. 2426–2432 (2018).

28. Liu, C., Cai, W., and Liu, L. "Hydrothermal carbonization synthesis of Al-pillared montmorillonite@ carbon composites as high performing toluene adsorbents", *Applied Clay Science*, **162**(June 2018), pp. 113–120 (2018).

29. Survey, U.G., Boden, T., and Tripp, B.T. "Gilsonite veins of the Uinta basin, Utah", *Utah Report No. 141 (Salt Lake: Utah Geological Survey)*, p. 50 (2012).

30. Jahanian, H.R., Shafabakhsh, G.H., and Divandari, H. "Performance evaluation of Hot Mix Asphalt (HMA) containing bitumen modified with Gilsonite", *Construction and Building Materials*, **131**, pp. 156–164 (2017).

31. Helms, J.R., Kong, X., Salmon, E., et al. "Structural characterization of gilsonite bitumen by advanced nuclear magnetic resonance spectroscopy and ultrahigh resolution mass spectrometry revealing pyrrolic and aromatic rings substituted with aliphatic chains", *Organic Geochemistry*, **44**, pp. 21–36 (2012).

32. Sutirman, Z.A., Sanagi, M.M., Karim, J.A., et al. "New crosslinked-chitosan graft poly (N-vinyl-2-pyrrolidone) for the removal of Cu(II) ions from aqueous solutions", *International Journal of Biological Macromolecules*, **107**, pp. 891–897 (2018).

33. Criado-Garcıa, L., Almofti, N., Arce, L., et al. "Photoionization-ion mobility spectrometer for non-targeted screening analysis or for targeted analysis coupling a Tenax TA column", *Sensors and Actuators B: Chemical*, **235**, pp. 370–377 (2016).

34. Deng, H., Pan, T., Zhang, Y., et al. "Adsorptive removal of toluene and dichloromethane from humid exhaust on MFI, BEA and FAU zeolites: An experimental and theoretical study", *Chemical Engineering Journal*, **394**(March), p. 124986 (2020).

35. Ding, E.X., Hussain, A., Ahmad, S., et al. "High-performance transparent conducting films of long single-walled carbon nanotubes synthesized from toluene alone", *Nano Research*, **13**(1), pp. 112–120 (2020).

36. Fang, P., Tang, Z.J.Z.X., Chen, X.B., et al. "Experimental study on the absorption of toluene from exhaust gas by paraffin/surfactant/water emulsion", *Journal of Chemistry*, **2016**, pp. 1–9 (2016).

37. Farsouni Eydi, E., Shariati, A., and Khosravi-Nikou, M.R. "Separation of BTEX compounds (benzene, toluene, ethylbenzene and xylenes) from aqueous solutions using adsorption process", *Journal of Dispersion Science and Technology*, **40**(3), pp. 453–463 (2019).

38. Jiang, N., Zhao, Y., Shang, K., et al. "Degradation of toluene by pulse-modulated multistage DBD plasma: Key parameters optimization through response surface methodology (RSM) and degradation pathway analysis", *Journal of Hazardous Materials*, **393**, p. 122365 (2020).

39. Tafreshi, N., Sharifnia, S., and Moradi Dehaghi, S. "Box-Behnken experimental design for optimization of ammonia photocatalytic degradation by ZnO/Oak charcoal composite", *Process Safety and Environmental Protection*, **106**, pp. 203–210 (2017).

40. Vahid, A., Qandalee, M., and Baniyaghoob, S. "H_2S removal using ZnO/SBA-3: New synthesis route and optimization of process parameters", *Scientia Iranica, Transactions C, Chemistry, Chemical Engineering*, **24**(6), pp. 3064–3073 (2017).

41. Yuan, Z., Xu, Z., Zhang, D., et al. "Box-Behnken design approach towards optimization of activated carbon synthesized by co-pyrolysis of waste polyester textiles and $MgCl_2$", *Applied Surface Science*, **427**, pp. 340–348 (2018).

42. Mourabet, M., El Rhilassi, A., El Boujaady, H., et al. "Removal of fluoride from aqueous solution by adsorption on apatitic tricalcium phosphate using Box-Behnken design and desirability function", *Applied Surface Science*, **258**(10), pp. 4402–4410 (2012).

43. Hazrati, N., Abdouss, M., Vahid, A., et al. "Removal of H_2S from crude oil via stripping followed by adsorption using ZnO/MCM-41 and optimization of parameters", *International Journal of Environmental Science and Technology*, **11**(4), pp. 997–1006 (2014).

44. Nciri, N., Song, S., Kim, N., et al. "Chemical characterization of gilsonite bitumen", *Journal of Petroleum & Environmental Biotechnology*, **5**(5), p. 1 (2014).

45. Javed, H., Luong, D.X., Lee, C.-G., et al. "Efficient removal of bisphenol-A by ultra-high surface area porous activated carbon derived from asphalt", *Carbon*, **140**, pp. 441–448 (2018).

46. Nakhaei, M., Naderi, K., Akbari, A., et al. "Moisture resistance study on PE-wax and EBS-wax modified warm mix asphalt using chemical and mechanical procedures", *Construction and Building Materials*, **189**, pp. 882–889 (2018).

47. Mirzaiyan, D., Ameri, M., Amini, A., et al. "Evaluation of the performance and temperature susceptibility of gilsonite-and SBS-modified asphalt binders", *Construction and Building Materials*, **207**, pp. 679–692 (2019).

48. Pakdaman, E., Osfouri, S., Azin, R., et al. "Synthesis and characterization of hydrophilic gilsonite fine particles for improving water-based drilling mud properties", *Journal of Dispersion Science and Technology*, **41**(11), pp. 1633–1642 (2020).

49. Zhou, L., Huang, W., Zhang, Y., et al. "Evaluation of the adhesion and healing properties of modified asphalt binders", *Construction and Building Materials*, **251**, p. 119026 (2020).

50. Naik, J., Rajput, R., and Singh, M.K. "Development and evaluation of ibuprofen loaded hydrophilic biocompatible polymeric nanoparticles for the taste masking and solubility enhancement", *Bio. Nano. Science*, pp. 1–11 (2020).

51. Akhtar, M., Saba, S., Arif, S., et al. "Efficient magnetoelectric dispersion in Ni and Co co-doped $BiFeO_3$ multiferroics", *Physica B: Condensed Matter*, p. 412572 (2020).

52. Jalilov, A.S., Li, Y., Tian, J., et al. "Ultra-high surface area activated porous asphalt for CO_2 capture through competitive adsorption at high pressures", *Advanced Energy Materials*, **7**(1), p. 1600693 (2017).

53. Rajisha, K.R., Deepa, B., Pothan, L.A., et al. "Thermomechanical and spectroscopic characterization of natural fibre composites", *Interface Engineering of Natural Fibre Composites for Maximum Performance*, pp. 241–274 (2011).

54. Araújo, C.S.T., Almeida, I.L.S., Rezende, H.C., et al. "Elucidation of mechanism involved in adsorption of Pb(II) onto lobeira fruit (Solanum lycocarpum) using Langmuir, Freundlich and Temkin isotherms", *Microchemical Journal*, **137**, pp. 348–354 (2018).

55. Ahmed, I. and Jhung, S.H. "Remarkable improvement in adsorptive denitrogenation of model fossil fuels with CuCl/activated carbon, prepared under ambient condition", *Chemical Engineering Journal*, **279**, pp. 327–334 (2015).

56. Ahmadi, M., Anvaripour, B., Khosravi-Nikou, M.R., et al. "Selective denitrogenation of model fuel through iron and chromium modified microporous materials (MSU-S)", *Journal of Environmental Chemical Engineering*, **5**(1), pp. 849–860 (2017).

57. Senthil Kumar, P., Ramalingam, S., Senthamarai, C., et al. "Adsorption of dye from aqueous solution by cashew nut shell: Studies on equilibrium isotherm, kinetics and thermodynamics of interactions", *Desalination*, **261**(1–2), pp. 52–60 (2010).

58. Farzin Nejad, N., Shams, E., Amini, M.K., et al. "Ordered mesoporous carbon CMK-5 as a potential sorbent for fuel desulfurization: Application to the removal of dibenzothiophene and comparison with CMK-3", *Microporous and Mesoporous Materials*, **168**, pp. 239–246 (2013).

59. Yu, F., Ma, J., Wang, J., et al. "Magnetic iron oxide nanoparticles functionalized multi-walled carbon nanotubes for toluene, ethylbenzene and xylene removal from aqueous solution", *Chemosphere*, **146**, pp. 162–172 (2016).

60. Bina, B., Amin, M.M., Rashidi, A., et al. "Water and wastewater treatment from BTEX by carbon nanotubes and nano-Fe", *Water Resources*, **41**(6), pp. 719–727 (2014).

61. Anjum, H., Johari, K., Gnanasundaram, N., et al. "A review on adsorptive removal of oil pollutants (BTEX) from wastewater using carbon nanotubes", *Journal of Molecular Liquids*, **277**, pp. 1005–1025 (2019).

62. Konggidinata, M.I., Chao, B., Lian, Q., et al. "Equilibrium, kinetic and thermodynamic studies for adsorption of BTEX onto Ordered Mesoporous Carbon (OMC)", *Journal of Hazardous Materials*, **336**, pp. 249–259 (2017).

63. Aivalioti, M., Pothoulaki, D., Papoulias, P., et al. "Removal of BTEX, MTBE and TAME from aqueous solutions by adsorption onto raw and thermally treated lignite", *Journal of Hazardous Materials*, **207**, pp. 136–146 (2012).

64. Jodeh, S., Ahmad, R., Suleiman, M., et al. "Kinetics, thermodynamics and adsorption of BTX removal from aqueous solution via date-palm pits carbonization using SPME/GC-MS", *Journal of Materials and Environmental Science*, **6**(10), pp. 2853–2870 (2015).

65. Daifullah, A.A.M.M. and Girgis, B.S. "Impact of surface characteristics of activated carbon on adsorption of BTEX", *Colloids and Surfaces A: Physicochemical and Engineering Aspects*, **214**(1–3), pp. 181–193 (2003).

66. Carvalho, M.N., Da Motta, M., Benachour, M., et al. "Evaluation of BTEX and phenol removal from aqueous solution by multi-solute adsorption onto smectite organoclay", *Journal of Hazardous Materials*, **239**, pp. 95–101 (2012).

Biographies

Arvin Saffarian Delkhosh received his BSc degree in Applied Chemistry from Tehran North Branch, Islamic Azad University, Tehran, Iran, 2014 and completed his MSc program in Analytical Chemistry at Science and Research Branch, Islamic Azad University, Tehran, Iran, in 2017. His research interests include synthesis and characterization of nanoporous materials, green chemistry, instrumental analysis, desulfurization and denitrogenation of model fuels, measurement of enzymatic activity, and electrochemical biosensors.

Amir Vahid received his BSc in Applied Chemistry from Razi University, Kermanshah, Iran, 2002 and his MSc and PhD both in Analytical Chemistry from the University of Mazandaran in 2006 and 2011, respectively. He is now an Assistant Professor at the Research Institute of Petroleum Industry and works on crude oil characterization and upgrading. His scientific interests include analytical chemistry, spectroscopy, oscillating chemical reactions, catalysis, adsorption, petroleum

chemistry, environmental pollution, synthesis and characterization of organic and inorganic porous materials and their application in the oil and gas industry on lab, bench, and pilot scales.

Sahar Baniyaghoob received her BSc in Pure Chemistry from Tehran University in 2003 as well as MSc and PhD in Inorganic Chemistry from Sharif University of Technology, Tehran, Iran, in 2005 and 2010, respectively. Dr. Baniyaghoob was on sabbatical leave from the University of Edinburgh, Edinburgh, UK. She is currently an Assistant Professor at Science and Research Branch, Islamic Azad University, Tehran, Iran. She is working in the field of inorganic chemistry with a special interest in the investigation of the interactions between Schiff base complexes, free radicals, metal-catalyzed reactions, and synthesis of biologically important molecules and macromolecules using UV-Vis spectroscopy. Furthermore, she uses the knowledge of chemistry in the oil industry, especially for applying useful techniques for desulfurization and upgrading of heavy oils.

Mohammad Saber-Tehrani received his BSc in Chemistry from Shiraz University, Fars, Iran in 1971. He obtained his MSc and PhD degrees in Analytical Chemistry from the University of Kent, Canterbury, UK in 1976 and 1981, respectively. Dr. Saber-Tehrani is presently an Assistant Professor of Analytical Chemistry at Science and Research Branch, Islamic Azad University, Tehran, Iran. His current research interests is extraction, environmental pollutant remediation, analytical chemistry instrumentation, and analytical method development and validation.